Journal of Power Sources 251 (2014) 195–201

Contents lists available at ScienceDirect

Journal of Power Sources

journal homepage: www.elsevier.com/locate/jpowsour

Realizing high visible-light-induced carriers mobility in TiO_2-based photoanodes

Jingfu He [a,1], Shibao Zhang [a,b,1], Zhihu Sun [a], Weiren Cheng [a], Qinghua Liu [a,*], Yong Jiang [a], Fengchun Hu [a], Zhiyun Pan [a], Bo He [a], Ziyu Wu [a], Wensheng Yan [a,*], Shiqiang Wei [a]

[a] National Synchrotron Radiation Laboratory, University of Science and Technology of China, Hefei, Anhui 230029, PR China
[b] Department of Physics, University of Science and Technology of China, Hefei, Anhui 230026, PR China

HIGHLIGHTS

- We successfully engineered the dopant energy states towards high carriers mobility.
- The split of the isolated band via N – S codoping favors to decrease the hole effective mass.
- The hole transport resistivity is decreased from 6.8 × 10^4 to 1.3 × 10^4 Ω m.
- The internal quantum efficiency increases from 5% to 20% at 450 –550 nm.

GRAPHICAL ABSTRACT

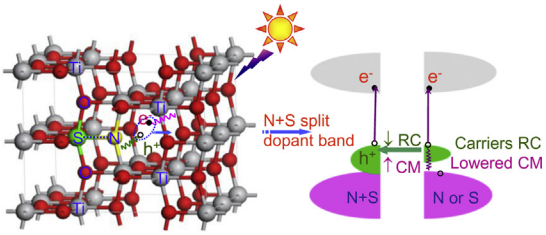

ARTICLE INFO

Article history:
Received 2 September 2013
Received in revised form
8 November 2013
Accepted 15 November 2013
Available online 1 December 2013

Keywords:
Titanium dioxide
Band structure engineering
Carrier mobility
Codoping
Visible light

ABSTRACT

Increasing the quantum conversion efficiency in visible-light region is a key issue for the efficient usage of solar energy in the process of photoelectrochemical (PEC) water splitting. Here, based on the N anion and S cation codoped TiO_2 thin film photoanodes, we find experimentally and theoretically that the transport ability of visible-light-induced carriers can be notably enhanced by engineering the dopant electronic energy states. The hole transport resistivity is decreased from 6.8 × 10^4 to 1.3 × 10^4 Ω m via delocalizing the introduced bands, leading to an evident increase of the internal quantum efficiency from 5% to 20% at the visible-light region of 450–550 nm. Further DFT calculations exhibit that the split of the isolated band is induced by a strong N and S hybridization, which favors to decrease the hole effective mass and to improve the hole mobility by three times. The photocurrent of N – S codoped TiO_2 thin film is thus twice that of monodoping cases, the best value for doping modified TiO_2 thin film photoanodes. This work may provide not only a design principle but also a candidate for tailoring and optimizing TiO_2 towards high PEC activity.

1. Introduction

Converting and storing solar energy in the form of hydrogen via photoelectrochemical (PEC) cells is one of the most promising ways for the production of clean and sustainable energy [1–6]. To realize the efficient conversion of solar light of PEC cells in practical application, semiconductors with high solar energy conversion efficiency and short energy payback time is highly required. Titanium dioxide (TiO_2) is one of the most potential photoanodes for hydrogen generation, due to its earth abundance, high chemical stability, and strong catalytic activity [7,8]. However, the large band gap (3.0 ~ 3.2 eV) of TiO_2 makes its relatively high reactivity only under ultraviolet (UV) light [9–14]. Great efforts have been paid to

* Corresponding authors. Tel.: +86 0551 63601997.
E-mail addresses: qhliu@ustc.edu.cn (Q. Liu), ywsh2000@ustc.edu.cn (W. Yan).
[1] These authors contributed equally to this work.

0378-7753/$ – see front matter © 2013 Elsevier B.V. All rights reserved.
http://dx.doi.org/10.1016/j.jpowsour.2013.11.057

extend the absorption of TiO_2 to cover the visible light region by doping/codoping with metal and/or nonmetal (NM) ions [15–23]. Unfortunately, the overall efficiency of solar-to-chemical energy for these materials is still quite low (around 1%), due to the poor utilization efficiency of visible-light-induced carriers via the modified band structure.

It is known that element doping in semiconductor could introduce dopant energy states within the band gap [7]. Recently, many researches have been performed to investigate the critical characters in introduced dopant energy states for visible light response and a series of models have been proposed for the construction of introduced energy states towards high wavelength light to chemical conversion efficiency. It has been recently recognized that a critical factor in determining the visible light response is the introduced band gap energy state. Therefore, how to tailor the introduced energy states towards high wavelength light is an essential issue in order to enhance the chemical conversion efficiency. Asahi et al. have first theoretically proposed the hypothesis that overlapping valence band and states in the band gap may help to transfer photoexcited carriers [8]. Using the first-principles calculations, Wei et al. have further promoted this concept to passivated codoping to avoid the existence of carrier recombination center [24]. Subsequently, the concept of passivated codoping is experimentally validated via Cr and Sb codoping, which obviously increases the lifetime of photocarriers compared to monodoping samples [25]. On the other hand, many researchers believe that noncompensated codoping models of anion–cation or double-hole-mediated are more easy to achieve high visible light absorption, which has been preliminarily confirmed by the 1.5 eV band gap in the Cr and N codoping case [26,27]. However, the quantum conversion efficiency in the visible-light regions for above models is still limited, typical lower than 10% at around 400–550 nm. The low efficiency is subsequently attributed to the inefficient visible-light excited carriers transport in these dopant energy states [28]. It is thus expected that the quantum conversion efficiency of the visible-light induced carriers could be obviously enhanced if the intermediate-dopant-bands were tailored to be efficient for carriers transport. Therefore, to improve the photocarriers' separation and transport abilities for improving solar conversion efficiency is of both scientific and technological importance.

In this work, we aim to increase the quantum conversion efficiency in the visible-light region of TiO_2-based photoanodes by engineering the dopant electronic energy states. We demonstrate that the mobility of photo-induced carriers in doping TiO_2 can be greatly improved by the degeneracy of impurity energy levels within the band gap of TiO_2 due to the controllable impurity level position of N anion and/or S cation doping. The hybridizing of N and S ions would split the isolated dopant energy band and result in a threefold increase of the hole mobility. Thus, the internal quantum efficiency at the region of 400–500 nm is enhanced to 22% and the photocurrent of (N + S)-codoping is twice the value of pure and monodoping TiO_2 samples. These findings could establish a guide for optimizing the doping/codoping of titania-based photocatalysts towards innovative solar energy conversion.

2. Experimental section

2.1. Sample synthesis

Single-crystalline TiO_2 and nonmetallic doped TiO_2 coated ITO glass samples were synthesized by sol–gel method. Briefly, tetrabutyl titanate was used as a starting material, ammonia as nitrogen source and sodium sulfite as sulfur source, respectively. All chemicals used in the experiments were of analytical reagent grade. 10 ml of tetrabutyl titanate and a certain amount of acetylacetone were mixed with 29.3 ml of ethanol and then stirred for 2 h to form solution A; 0.9 g of sodium sulfite (atomic ratio of S/Ti = 0.25) and 6 ml of ammonia were added into the mixture solution of 14.6 ml of ethanol and 40 ml of ultrapure deionized water to form solution B. Solution B was added dropwise into solution A under vigorously stirring condition. After continuous stirring for 2 h, the mixture sol solution was then left to stand for 3–5 days. The glasses were unltrasounded for 30 min each in acetone, ethanol and deionized water, and then placed on the spin coater. The sol solution was dipped on the glass at low spin speed of 300 rad s^{-1}. Following that the spin speed was promoted to 3000 rad s^{-1} to uniform the coating layer of sol solution. The coated TiO_2 ITO glass was then placed in a 333 K oven for 10 min and followed by the next spin-coating dipping process. Five spin-coating dipping processes are performed and the thickness of TiO_2 thin films is about 800 nm. After calcination at 823 K for 2 h, (N + S)-codoped TiO_2 electrodes were prepared. For comparison, undoped TiO_2, N-doped TiO_2, and S-doped TiO_2 photoelectrodes were synthesized respectively by a similar procedure.

2.2. Structure and photocatalysis characterization

The powder x-ray diffraction (XRD) patterns of the samples were recorded using Cu $K\alpha$ ($\lambda = 0.154$ nm) radiation in the 2θ range from 20° to 80°. UV–vis absorption spectra were collected using the diffuse reflection mode with the Shimadzu SolidSpec-3700 UV–vis spectrometer. Synchrotron radiation photoelectron spectroscopy experiments were performed at National Synchrotron Radiation Laboratory (NSRL), China. Electrochemical measurements were carried out using an electrochemical workstation (Model CHI760D, CH instruments, Inc., Austin, TX) with a three-electrode system, which was operated with the TiO_2 sample as anode, platinum mesh as cathode, and Ag/AgCl as reference electrode. The curves of potential dependence of the current density were measured using linear sweep voltammograms (LSV) from −1.0 to 0.6 V at a scan rate of 0.002 V s^{-1}. Electrochemical impedance spectroscopy (EIS) measurements were carried out with frequency range of 0.01–100 kHz at different bias potentials in different pH values and stirring solutions. All potential values in this work are reported with respect to the Ag/AgCl reference. The irradiation source is a 300 W Xe lamp with AM1.5 simulator and the monochromatic light is filtered by filter plates of different wavelengths with bandwidth of 10 nm and transmittance of 80%. The monochromatic light power density is measured by UV–visible irradiatometer with the accuracy of 1 μW cm^{-2}. All of the photocurrent values are calibrated to the incident energy density of 100 mW cm^{-2}.

2.3. Computational details

The first-principles total-energy and band structure calculations were performed within the generalized gradient approximation (GGA) as implemented in the VASP code [29–31]. The electron and core interactions were described using the frozen-core projector-augmented-wave (PAW) method [32]. To overcome the well-known band gap limitations in density functional theory (DFT), the GGA + U method was used to treat the Ti 3d electrons ($U = 3.0$ eV and $J = 0.87$ eV), producing an intrinsic band gap of 3.2 eV. The wave function was expanded in plane waves with a cutoff energy of 400 eV. For all the doped systems, a 48-atom $2 \times 2 \times 1$ supercell was employed. The Brillouin zone integrations for total-energy calculations were performed using the k-points that are equivalent to the $5 \times 5 \times 5$ Monkhorst-Pack k-point meshes [33], more refined $7 \times 7 \times 7$ k-point meshes were used for the density of states (DOS) plots.

3. Results and discussion

Fig. 1a shows that the visible light response of (N + S) codoped TiO_2 thin film is distinctly stronger than that of N or S monodoping. The photocurrent values for N or S monodoped TiO_2 at −0.4 V are 0.067 and 0.087 mA cm^{-2}, respectively. Strikingly, the photocurrent of (N + S)-codoped TiO_2 is dramatically increased to 0.36 mA cm^{-2}, about five times higher than those of the monodoped cases. The electronic properties of these samples under visible light radiation also show a great difference from electrochemical impedance spectroscopy (Fig. 1b). From the inset of Fig. 1b, it can be obtained that there exists a transmission line for all of the doping TiO_2 electrodes, which implies the strong impact of carrier transport obstruction based on the recently established theory of impedance of finite-diffusion porous electrodes [34,35]. The equivalent circuit was also shown in Fig. 1b, where r_{tr}, r_{ct}, and C' represent the distributed component of the transport resistance R_{tr}, the charge transfer resistance R_{ct}, and the capacitance of the TiO_2/electrolyte interface C, respectively. It is known that the value of transport resistance R_{tr} can be directly read as three times of the projection of transmission line on X axis as marked in the inset of Fig. 1b. The R_{tr} of S doping, N doping, and codoping TiO_2 obtained by this method are 570 Ω, 530 Ω, and 110 Ω, respectively. Therefore, the carrier transport resistance for the codoped sample is about 5 times smaller than that for the monodoped samples. In the previous researches, N and S are always choosen as candidates for TiO_2 modification to extend the valence band. However, their photocurrent contribution from visible light radiation is still small (less than 0.1 mA cm^{-2} at −0.4 V vs Ag/AgCl) [36–38], similar to our experimental results of N and S monodoped TiO_2 films. As for the other common treating methods such as hydrogen reduction, the visible light region photoresponse is even much lower, although the introduced absorption is fascinating [39]. It is generally considered that the poor energy conversion efficiency is originated from the hindered carrier transport, which is confirmed by our EIS analysis. Here, one of the best visible light photocurrents of 0.36 mA cm^{-2} for TiO_2 thin films is achieved in a (N + S) codoped TiO_2 that dramatic decreases the transport resistance, indicating the efficient engineering of electronic energy states via (N + S) codoping.

To directly analyze the characters of dopants energy states that are responsible for these amazing differences, UV-photoelectron spectroscopy (UPS) are performed with the measured results shown in Fig. 1c. N or S doping alone creates only localized electronic states in the band gap (indicated by dot rectangle), in agreement with the reported results [15,40]. It is of high interest that upon (N + S)-codoping, the dopant energy states are remarkably hybridized to form broad continuum bands. The positions of introduced band of monodoped and codoped TiO_2 samples are almost the same since they are originated from the same dopants. The presence of sulfur and nitrogen in titania was identified from the X-ray photoelectron spectroscopy (XPS) results as shown in Fig. 2a. The Ti 2p and the O 1s peaks are located at 458.9 eV and 530.1 eV, respectively, consistent with the previous report [41]. The minor change of Ti and O chemical environment might result from the comparably lower concentrations of N and S doping. The N 1s characteristic peak at 397.6 eV is consistent with that for the lattice nitrogen (N–Ti–N) and is completely different from the cationic N (~405 eV) and interstitial site N with chemical environment of Ti–N–O (~400 eV) [8,40,42]. On the other hand, S 2p3/2 peak is located at 169.0 eV, corresponding to the S ions (+6) surrounded by O ions [43]. It is worth noting that there was a little hump on the high energy side of O 1s spectra which might result from the S–O bonding, since the electronegativity of S is stronger than Ti. All the above results pointed towards the occupation of cation and anion sites in the lattice for S and N atoms, respectively. The broad continuum bands just above the valence band maximum of N − S codoped TiO_2 is likely to result from the interaction between N^{3-} and S^{6+} ions. X-ray diffraction (XRD) patterns and Scanning Electron Microscope (SEM) (Fig. 2b) results further confirmed that the phase and morphology of TiO_2 thin films are

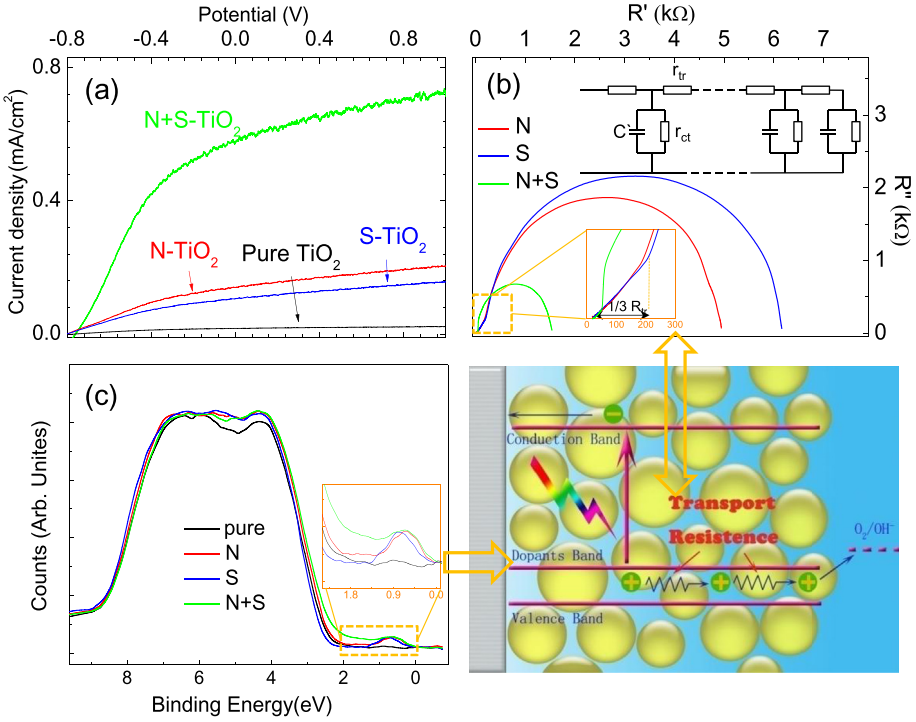

Fig. 1. (a) The Current density under visible light radiation (>400 nm) of pure-, N-, S-, and (N + S)-TiO_2 thin films. (b) Nyquist plots of N-, S-, and (N + S)-TiO_2 thin films. (c) UPS of pure-, N-, S-, and (N + S)-TiO_2 thin films. The inset of (b) is the equivalent circuit of transmission line model with the relationships of $R_{ct} = r_{ct}/L$ and $R_{tr} = r_{tr}{}^{*}L$.

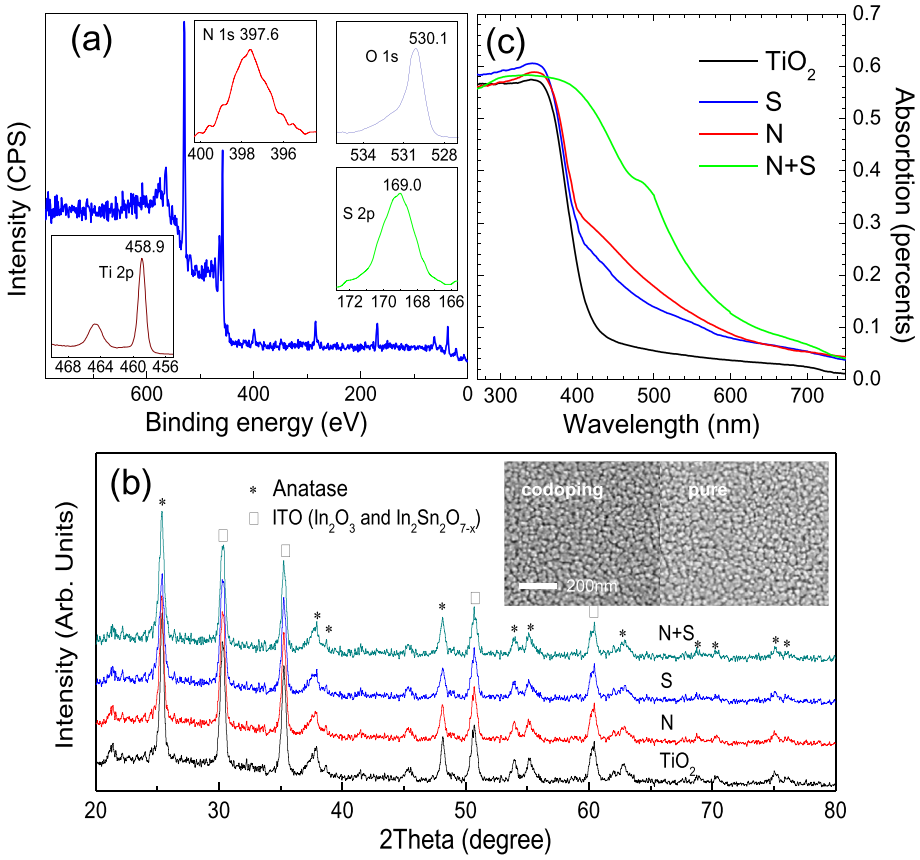

Fig. 2. (a) XPS survey of (N + S)-TiO_2 thin film, the insets of (a) are XPS spectra of O, Ti, N and S in (N + S)-TiO_2 thin films. (b) XRD of pure-, N-, S-, and (N + S)-TiO_2 thin films, the insets of (b) are SEM of codoping and pure TiO_2 thin films. (c) UV–visible absorption spectra of pure-, N-, S-, and (N + S)-TiO_2 thin films.

identical for all doped samples. These confirm that the only difference of electronic energy states of doped TiO_2 samples are the widths of dopants band. The optical absorption for these N and/or S doped TiO_2 electrodes (as shown in Fig. 2c) correspond to the UPS results, with an obvious absorption tail to 600 nm as the results of the extra transition from the dopant energy level to conduction band with the energy difference of 2.1 eV. The larger absorption coefficient for codoped sample is consistent with the larger density of energy states. The difference of absorption coefficient for monodoped and codoped samples are obviously smaller than the changes of transport resistance and photocurrent values, indicating that the enhancement of carrier mobility is the main reason for the reduction of carrier transport resistance. These above observations suggest that broadening and splitting dopants energy states would increase the carrier mobility on the dopants band and improve the energy conversion efficiency.

The variation of surface reaction activity induced by the dopants modification is also a possible influence. The contribution of (N + S) hybridization on surface reaction rate is investigated through the comparison of photocurrent with and without 0.5 M hydrogen peroxide, which is an easily oxidized holes scavenger to completely suppress surface recombination [44]. The saturated photocurrent values of codoped and monodoped samples are both increased by about 10%, indicating surface reaction is not a major hinder in the PEC process of pure and doped TiO_2 thin films. It is worth noting that the change ratios between codoped and monodoped samples are all the same, as shown in Fig. 3a and b, indicating that the surface reaction activity is not changed. The chopped light chronoamperometry measurement results (inset of Fig. 3b) further confirm that the surface charge accumulation and recombination are identical for all doped TiO_2 samples. Thus, the different utilization ratios of visible-light induced carriers in different samples are totally originated from the transport mobility.

To further quantitatively analyze the relationship between the PEC activity and the characters of dopant level, we anatomize the monochromatic light PEC activity of the samples using the concept of internal quantum efficiency (IQE) with formula to normalize the absorption coefficient [45]:

$$\mathrm{IQE} = \frac{I(\mathrm{mA\ cm^{-2}}) \times [1240/\lambda(\mathrm{nm})]}{A \times P(\mathrm{mW\ cm^{-2}})} \quad (1)$$

I is the photocurrent density at −0.4 V vs Ag/AgCl, and A is the absorption ratio. As shown in Fig. 3c, all the doped TiO_2 thin films present improved visible monochromatic light photoconversion efficiency relative to pure TiO_2, because of the enhanced visible absorption by doping foreign elemental species in TiO_2 host lattice. However, the utilization rates of visible-light-induced carriers are extremely different. For the two monodoped samples, the IQE at visible light region of 400–500 nm are quickly decreased from 15% to 5%, similar to the previous reports of N-doped TiO_2 photoanodes [36,37]. It is exciting that the IQE for the codoped sample forms a plateau with the values around 23% from 400 nm to 500 nm and remains 8% at 550 nm. In the doped TiO_2, visible-light-excited an electron into the conduction band, leaving photogenerated holes in impurity levels. Therefore, the diverse usage efficiency of visible light for different kind of dopant levels is originated from the transfer efficiency of hole carriers on the impurity level. The plateau of IQE for the codoped sample suggests that the broad energy band provides sufficient carrier transport ability for the hole carriers. To

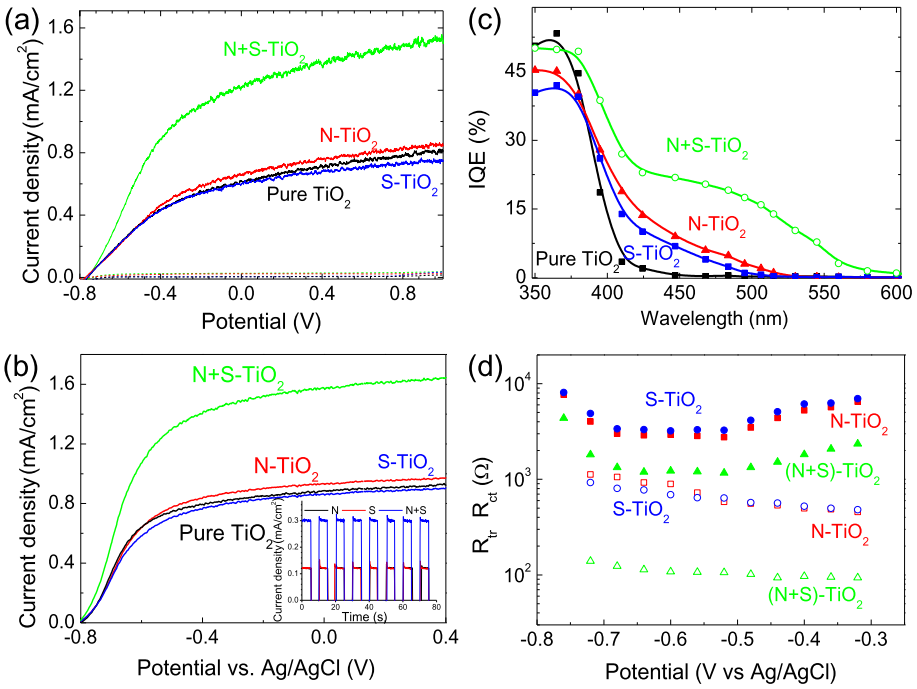

Fig. 3. The Current density in (a) 1 M KOH solution, (b) 1 M KOH contained 0.5 M H_2O_2 solution under AM1.5 radiation of pure-, N-, S-, and (N + S)-TiO_2 thin films. (c) IQE curves of pure-, N-, S-, and (N + S)-TiO_2 thin films. (d) The R_{tr} (hollow dots) and R_{ct} (solid dots) for N (square), S (circle), and (N + S) codoping (triangle) TiO_2 thin films.

analyze the variation of resistance in depth, the values for the parameters of R_{tr} and R_{ct} from EIS data at −0.4–0.4 V under visible light radiation are plotted in Fig. 3d. The value of R_{tr} is determined as three times of the projection of transmission line on X axis, and the value of R_{ct} equals to the diameter of the semicircular at low frequencies. The sustained decreasing of R_{ct} values is due to the surface band curving, which boosts the carrier transport in the bulk and also provides larger overpotential for the surface reaction. In the whole voltage region, the R_{tr} for the codoped sample is 5 times smaller than that for the monodoped one. Taking into account the film thickness of 800 nm, the hole transport resistivity of N, S monodoping and codoping are about $7 \times 10^4\ \Omega$ m, $6 \times 10^4\ \Omega$ m and $1.3 \times 10^4\ \Omega$ m, respectively, consistent with the resistivity of semiconductor (10^{-4}–$10^7\ \Omega$ m). The comparable high resistivity of the dopants energy band demonstrate important role of decreasing transport resistance for the band structure engineering. The hole mobility can be simulated by the following formula [46]:

$$R_{tr} = \frac{d_{film}}{\sigma} = \frac{d_{film}}{qp\mu} \tag{2}$$

where d_{film} is the film thickness and the conductivity σ is determined by the product of the hole mobility μ_p, and the hole concentration p. Since the intrinsic charge density is comparable lower, the hole concentration might mainly contributed by the photon excitation ($\sim 6 \times 10^{22}\ cm^{-3}s^{-1}$). The light absorption of codoping is doubled compared to the monodoping, indicating that the hole mobility of continuum energy states are at least increase by 2–3 times for (N + S) codoping.

Since the charge migration properties are strongly dependent on the electronic structure, the theoretical calculations are carried out to elucidate the origin of the changes in the electrochemical properties of (N + S)-modified TiO_2. The XPS results have shown that N and S occupy the anionic and cationic sites in anatase titania, and that the doped concentration are about 1%–2%. The structure model for the calculation is thus shown in Fig. 4. The formation energies of different occupation sites are previously calculated following the formulation described elsewhere [19,20], and the cation–anion model is indeed energetically most favored, which also constituted strong evidence for the validity of DFT calculation. For N- and S-monodoped TiO_2 cases, the calculated total density of states (TDOS) and projected DOS (PDOS) in Fig. 4b and d show that the impurity states are strongly localized within the band gap without altering both the VBM and conduction band minimum (CBM). Whereas in the case of (N + S)-codoped TiO_2, some different features could be found from their TDOS and PDOS as shown in Fig. 4e. Since both of N and S atoms are as NM elements, the p–p interactions between O and N/S atoms intensify the hybridization of VB with (N + S) states. Thus, we can find that the former isolated band gap energy level is merged into a broad continuum bands, and overlap with the VB, in good agreement with our experiments. It is worth noting that (N + S)-codoping makes a significant increase of IQE in visible light region compared with that of N or S monodoping. This indicates an increase of carrier mobility which can be deduced by a semi-quantitative evaluation of the carrier mobility for these models. The carrier mobility μ can be expressed as

$$\mu = q\tau/m^* \tag{3}$$

where q and τ are the electric quantity and average lifetime of the carrier, respectively, and m^* the carrier effective mass [47]. Given a similar τ for the same type of carriers in the TiO_2-based systems, the carrier mobility is inversely proportional to m^*. It is known that m^* is inversely proportional to the curvature of the VB top (k_t) and can be roughly calculated via the density of states:

$$g_v(E) = \frac{8\pi\sqrt{2}}{h^3} m_h^{*3/2} \sqrt{E_v - E} \tag{4}$$

By comparing the top region (about 0.1 eV wide as shown in the inset of Fig. 4b, d, e) of dopants energy states in monodoping and codoping cases, the k_t for the codoping case is estimated to be approximately 3 times larger than monodoping cases, owing to the

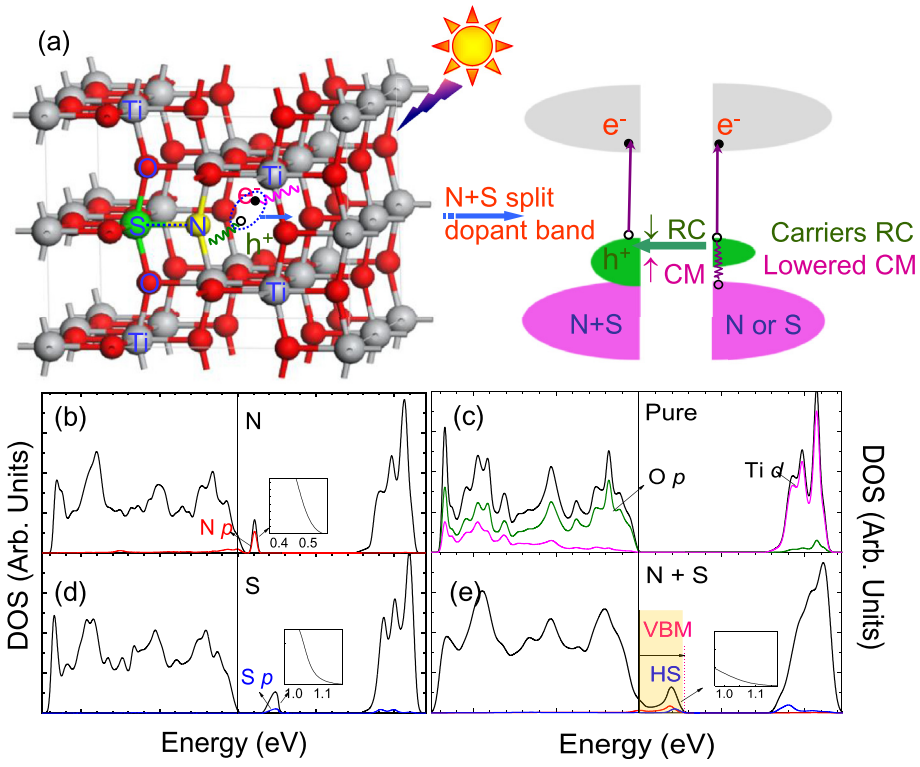

Fig. 4. (a) Model structure for defective anatase TiO_2 showing the location of the dopants. Ion doping sites are marked with N and S. RC and CM are the abbreviations of "recombination center", and "carriers mobility", respectively. "↓" and "↑" mean "decrease" and "increase", respectively. The calculated TDOSs and PDOSs for (b) N and (d) S-monodoped, (c) pure TiO_2 and (e) (N + S)-codoped TiO_2. The energy is measured from the VBM of pure TiO_2. The insets are magnified plots of the VB tops.

delocalization of impurity bands. Therefore, the carrier mobility of the (N + S)-doped TiO_2 rises correspondingly by more than 300% compared with the monodoping, consisting with the experimental results. Hence, these results suggest that the improvement of quantum conversion efficiency for (N + S)-codoped TiO_2 could be attributed to the enhanced charge carriers mobility.

For the researches of all these years, dopants with donor or acceptor levels are introduced into the crystal of TiO_2 to obtain the high visible light absorption. The photogenerated carrier would be localized by the dopant ion as an isolated energy state unless the concentration of dopant ion is above 10^{17} and the dopant energy band would be formed. This extra energy band can also be efficient for the carriers transport, however, it is worth noting that the electrochemical properties of the extra energy band are very different from the intrinsic band. In most cases, the newly introduced energy band are poor channel for the carrier transport. Just as our EIS results exhibited, the transport resistance for monodoping is 500–600 ohms for the thin films of 800 nm, which is a common thickness for TiO_2 and other transition metal oxide photoanode. These would cause a voltage drop of 0.5–0.6 V for the photocurrent value of 1 mA cm^{-2} and performance recession of 50%. Any slight enhancement of carrier transport would greatly increase the energy conversion efficiency. Thus, it is very important to establish a standard for the construction of extra energy level with high hole mobility. Our research exhibits that the carrier mobility is strongly related with the breadth of the dopant level, and the suppression of degeneracy and localization of dopant level would greatly benefit the carriers mobility. Step further, the large curvature of the VB top could ensure that the carriers gain more energy and velocity while migrating in the periodic potential field. This conclusion is also coincident with the researches of mobility enhancement in strained Si MOSFETs [48], in which the effect of strain would split the six-fold degenerated conduction band, resulting in the decrease of electron effective mass and increase the electron mobility. N and S monodoping are the most common approaches for the tailoring the valence band maximum. However, the monodoping samples with doping concentration of 1%–2% in our experiments show that the introduced energy states are isolated. This indicated that the interaction between dopant ions are weak and the degeneration is still strong, resulting in a low carrier mobility. Theoretically, further increasing the doping concentration would lead to the band broadening, but it is fairly difficult to achieve in the experiment. On the other hand, the N and S coupling in codoping TiO_2 would be easily hybridized and split the dopant band to decrease the carrier effective mass. The utilization rate of excited electron–hole pairs is greatly enhancement, resulting in the energy conversion efficiency of 3% around 500 nm. It is worth mentioning that, other benefit may be also brought by the (N + S) codoping: (1) reducing the effective band gap to ~2.1 eV, (2) the Fermi level of (N + S)-TiO_2 is tuned inside the energy gap, and (3) the photocarriers trapping arising from the charged states around the Fermi surface is effectively confined. In this study, we not only demonstrated an important criterion for the building of efficient energy level, but also provided an example to meet the demands, which would provide a certain foundation for the future design of efficient photoelectrode.

4. Conclusion

In summary, a route of engineering the dopant electronic energy states in (N + S)-codoped TiO_2 is presented to improve the charge mobility and separation probability of the visible-light-excited electron–hole pairs. It is demonstrated that the transport of visible-light induced holes is more favored on the continuum

energy states of (N + S) codoping than on the isolated energy states of N or S monodoping, resulting in fivefold increase of the absorbed photon to chemistry quantum efficiency in the visible-light region of 450–550 nm. Further analyses via electrochemical impendence spectra and first-principles calculations show that the hole mobility is increased by three times after the hybridizing of N and S dopant levels, which is responsible for the significantly increased quantum conversion efficiency and visible-light driven photocurrent. These results provide an important principle for the further tailoring of the band structure of TiO_2 via element doping towards high photoelectrochemical activity.

Acknowledgments

This work was supported by the National Natural Science Foundation of China (Grant Nos. 11135008, 11105151, 11305174, U1332111, and 11079004), the National Basic Research Program of China (2012CB825800), the Science Fund for Creative Research Groups of NSFC (11321503), and the Fundamental Research Funds for the Central Universities (WK2310000014, WK2310000023, and WK2310000030). The authors would like to thank NSRL, BSRF, and SSRF for the synchrotron radiation beamtime.

References

[1] M.G. Walter, E.L. Warren, J.R. McKone, S.W. Boettcher, Q.X. Mi, E.A. Santori, N.S. Lewis, Chem. Rev. 110 (2010) 6446–6473.
[2] T.R. Cook, D.K. Dogutan, S.Y. Reece, Y. Surendranath, T.S. Teets, D.G. Nocera, Chem. Rev. 110 (2010) 6474–6502.
[3] A. Fujishima, K. Honda, Nature 238 (1972) 37–38.
[4] M.R. Hoffmann, S.T. Martin, W.Y. Choi, D.W. Bahnemann, Chem. Rev. 95 (1995) 69–96.
[5] M. Gratzel, Nature 414 (2001) 338–344.
[6] A.I. Hochbaum, P.D. Yang, Chem. Rev. 110 (2010) 527–546.
[7] G. Liu, L.Z. Wang, H.G. Yang, H.M. Cheng, G.Q. Lu, J. Mater. Chem. 20 (2010) 831–843.
[8] R. Asahi, T. Morikawa, T. Ohwaki, K. Aoki, Y. Taga, Science 293 (2001) 269–271.
[9] T.L. Thompson, J.T. Yates, Chem. Rev. 106 (2006) 4428–4453.
[10] X. Chen, S.S. Mao, Chem. Rev. 107 (2007) 2891–2959.
[11] J. Zhang, Q. Xu, Z. Feng, M. Li, C. Li, Angew. Chem. Int. Ed. 47 (2008) 1766–1769.
[12] K. Lee, D. Kim, P. Roy, I. Paramasivam, B.I. Birajdar, E. Spiecker, P. Schmuki, J. Am. Chem. Soc. 132 (2010) 1478–1479.
[13] S.P. Albu, A. Ghicov, S. Aldabergenova, P. Drechsel, D. LeClere, G.E. Thompson, J.M. Macak, P. Schmuki, Adv. Mater. 20 (2008) 4135–4139.
[14] Y.F. Ji, B. Wang, Y. Luo, J. Phys. Chem. C 116 (2012) 7863–7866.
[15] X.B. Chen, C. Burda, J. Am. Chem. Soc. 130 (2008) 5018–5019.
[16] G. Liu, H.G. Yang, X.W. Wang, L.N. Cheng, J. Pan, G.Q. Lu, H.M. Cheng, J. Am. Chem. Soc. 131 (2009) 12868–12869.
[17] J. Wang, D.N. Tafen, J.P. Lewis, Z.L. Hong, A. Manivannan, M.J. Zhi, M. Li, N.Q. Wu, J. Am. Chem. Soc. 131 (2009) 12290–12297.
[18] J. Choi, H. Park, M.R. Hoffmann, J. Phys. Chem. C 114 (2010) 783–792.
[19] J.F. He, Q.H. Liu, Z.H. Sun, W.S. Yan, G.B. Zhang, Z.M. Qi, P.S. Xu, Z.Y. Wu, S.Q. Wei, J. Phys. Chem. C 114 (2010) 6035–6038.
[20] Y.H. Peng, J.F. He, Q.H. Liu, Z.H. Sun, W.S. Yan, Z.Y. Pan, Y.F. Wu, S.Z. Liang, W.R. Cheng, S.Q. Wei, J. Phys. Chem. C 115 (2011) 8184–8188.
[21] P. Roy, S. Berger, P. Schmuki, Angew. Chem. Int. Ed. 50 (2011) 2904–2939.
[22] L. Zhao, X.F. Chen, X.C. Wang, Y.J. Zhang, W. Wei, Y.H. Sun, M. Antonietti, M.M. Titirici, Adv. Mater. 22 (2010) 3317–3321.
[23] R. Shirley, M. Kraft, O.R. Inderwildi, Phys. Rev. B 81 (2010) 075111.
[24] Y.Q. Gai, J.B. Li, S.S. Li, J.B. Xia, S.H. Wei, Phys. Rev. Lett. 102 (2009) 036402.
[25] T. Ikeda, T. Nomoto, K. Eda, Y. Mizutani, H. Kato, A. Kudo, H. Onishi, J. Phys. Chem. C 112 (2008) 1167–1173.
[26] W.G. Zhu, X.F. Qiu, V. Iancu, X.Q. Chen, H. Pan, W. Wang, N.M. Dimitrijevic, T. Rajh, H.M. Meyer, M.P. Paranthaman, G.M. Stocks, H.H. Weitering, B.H. Gu, G. Eres, Z.Y. Zhang, Phys. Rev. Lett. 103 (2009) 226401.
[27] W.J. Yin, S.H. Wei, M.M. Al-Jassim, Y.F. Yan, Phys. Rev. Lett. 106 (2011) 066801.
[28] F.C. Wu, H.P. Lan, Z.Y. Zhang, P. Cui, J. Chem. Phys. 137 (2012) 104702.
[29] J.P. Perdew, Y. Wang, Phys. Rev. B 45 (1992) 13244.
[30] G. Kresse, J. Furthmuller, Phys. Rev. B 54 (1996) 11169.
[31] G. Kresse, J. Furthmuller, Comput. Mater. Sci. 6 (1996) 15.
[32] P.E. Blochl, Phys. Rev. B 50 (1994) 17953.
[33] H.J. Monkhorst, J.D. Pack, Phys. Rev. B 13 (1976) 5188.
[34] J. Bisquert, J. Phys. Chem. B 106 (2002) 325–333.
[35] F.F. Santiago, E.M. Barea, J. Bisquert, G.K. Mor, K. Shankar, C.A. Grimes, J. Am. Chem. Soc. 130 (2008) 11312–11316.
[36] S. Hoang, S.W. Guo, N.T. Hahn, A.J. Bard, C.B. Mullins, Nano Lett. 12 (2012) 26–32.
[37] A. Ghicov, J.M. Macak, H. Tsuchiya, J. Kunze, V. Haeublein, L. Frey, P. Schmuki, Nano Lett. 6 (2006) 1080–1082.
[38] X.H. Tang, D.Y. Li, J. Phys. Chem. C 112 (2008) 5405–5409.
[39] G.M. Wang, H.Y. Wang, Y.C. Ling, Y.C. Tang, X.Y. Yang, R.C. Fitzmorris, C.C. Wang, J.Z. Zhang, Y. Li, Nano Lett. 11 (2011) 3026–3033.
[40] M. Batzill, E.H. Morales, U. Diebold, Phys. Rev. Lett. 96 (2006) 026103.
[41] R. Liu, W.D. Yang, L.S. Qiang, J. Power Sources 199 (2012) 418–425.
[42] M. Sathish, B. Viswanathan, R.P. Viswanath, C.S. Gopinath, Chem. Mater. 17 (2005) 6349–6353.
[43] T. Ohno, T. Mitsui, M. Matsumura, Chem. Lett. 32 (2003) 364–365.
[44] H. Dotan, K. Sivula, M. Gratzël, A. Rothschild, S.C. Warren, Energy Environ. Sci. 4 (2011) 958–964.
[45] K. Shankar, J.I. Basham, N.K. Allam, O.K. Varghese, G.K. Mor, X.J. Feng, M. Paulose, J.A. Seabold, K.S. Choi, C.A. Grimes, J. Phys. Chem. C 113 (2009) 6327–6359.
[46] C.Y. Cummings, F. Marken, L.M. Peter, K.G.U. Wijayantha, A.A. Tahir, J. Am. Chem. Soc. 134 (2012) 1228–1234.
[47] C. Kittel, Introduction to Solid State Physics, Wiley, New York, 1976.
[48] K.K. Rim, J.L. Hoyt, J.F. Gibbons, IEEE Trans. Electron Dev. 47 (2000) 1406–1415.